DEVELOPMENT OF PREDICTIVE REACTION MODELS OF SOOT FORMATION

Final Technical Report

(Grant No. AFOSR 91-0129)

Covering the period from January 1, 1991 to December 31, 1993

prepared for

AIR FORCE OFFICE OF SCIENTIFIC RESEARCH
Bolling AFB

by

Michael Frenklach
Fuel Science Program
Department of Materials Science and Engineering
The Pennsylvania State University
University Park, PA 16802

February 9, 1994

REPORT DOCUMENTATION PAGE

Form Approved
OMB No. 0704-0188

1. AGENCY USE ONLY (Leave blank)

2. REPORT DATE
February 9, 1994

3. REPORT TYPE AND DATES COVERED
Final Technical Report

4. TITLE AND SUBTITLE
(U) Development of Predictive Reaction Models of Soot Formation

5. FUNDING NUMBERS
PE - 61102F
PR - 2308
SA - BS
G - AFOSR 91-0129

6. AUTHOR(S)

Michael Frenklach

7. PERFORMING ORGANIZATION NAME(S) AND ADDRESS(ES)
The Pennsylvania State University
University Park, PA 16802

8. PERFORMING ORGANIZATION REPORT NUMBER

AEOSR-TR- 94 0186

9. SPONSORING/MONITORING AGENCY NAME(S) AND ADDRESS(ES)
AFOSR/NA
110 Duncan Avenue, Suite B115
Bolling AFB DC 20332- 0001

10. SPONSORING/MONITORING AGENCY REPORT NUMBER

11. SUPPLEMENTARY NOTES

12a. DISTRIBUTION/AVAILABILITY STATEMENT

Approved for public release; distribution is unlimited

12b. DISTRIBUTION CODE

13. ABSTRACT (Maximum 200 words)

The ultimate objective of the present research program is to develop a predictive reaction model for soot formation in hydrocarbon flames. The principal accomplishments in the reported period are: (1) A computer algorithm was developed that calculates optical properties of an ensemble of particles whose size distribution is given in terms of moments of the size distribution function. (2) A computational study of sooting limits in laminar premixed flames was initiated and completed. It was found that the critical equivalence ratios for soot appearance, both the absolute values and temperature dependencies, can be predicted fairly close to the experimental observations. (3) New estimation techniques were developed and applied for calculations of standard-state enthalpies of formation and binary gaseous diffusion coefficients of polycyclic aromatic hydrocarbons (PAHs) and their radicals, thus providing critical information for accurate modeling of soot formation in flames. (4) Theoretical studies of a bench-mark ion-molecule reaction were initiated and completed. The results obtained further support the neutral-species reaction pathway as the predominant route for the formation and growth of PAHs, the precursors to soot in hydrocarbon flames. (5) A computational study of pressure effect on soot formation was performed. (6) A reduced model for PAH and soot formation in turbulent reactive flows was developed.

14. SUBJECT TERMS

Soot Formation, Reaction Mechanisms, Modeling

15. NUMBER OF PAGES
30

16. PRICE CODE

17. SECURITY CLASSIFICATION OF REPORT	18. SECURITY CLASSIFICATION OF THIS PAGE	19. SECURITY CLASSIFICATION OF ABSTRACT	20. LIMITATION OF ABSTRACT
Unclassified	Unclassified	Unclassified	UL

TABLE OF CONTENTS

INTRODUCTION

The ultimate objective of the present research program is to develop a predictive reaction model for soot formation in hydrocarbon flames. The specific objectives of the proposed 3-year study were: 1) To extend the modeling efforts to computer simulation and analysis of more complex sooting phenomena, such as sooting limits in laminar premixed flames; and 2) Further refinement of the underlying reaction mechanism of soot formation.

ACCOMPLISHMENTS

The principal accomplishments of the past three years, under the support of this grant, are the following:

- A computer algorithm was developed that calculates optical properties of an ensemble of particles whose size distribution is given in terms of moments of the size distribution function. The new algorithm allows us to simulate light absorption and scattering without assuming a functional form for the particle size distribution, and thus to compare directly the numerical predictions of the model to the actual measured properties, such as intensity of scattered light determined by laser diagnostics.
- A computational study of sooting limits in laminar premixed flames was initiated and completed. It was found that the critical equivalence ratios for soot appearance, both the absolute values and temperature dependencies, can be predicted fairly close to the experimental observations. Sensitivity and reaction-path analyses were performed to examine the factors responsible for the computed behavior.
- New estimation techniques were developed and applied for calculations of standard-state enthalpies of formation and binary gaseous diffusion coefficients of polycyclic aromatic hydrocarbons (PAHs) and their radicals, thus providing critical information for accurate modeling of soot formation in flames.
- Theoretical studies of a bench-mark ion-molecule reaction were initiated and completed. The results obtained further support the neutral-species reaction pathway as the predominant route for the formation and growth of PAHs, the precursors to soot in hydrocarbon flames.
- A computational study of pressure effect on soot formation was performed.
- A reduced model for PAH and soot formation in turbulent reactive flows was developed.

The results obtained are detailed below; for those that already appeared in the published form only brief descriptions are given, and for those yet not published, a more detailed account is provided.

RESULTS

Detailed Simulation of Sooting Limits in Laminar Premixed Flames[1]

The critical equivalence ratios were determined for several atmospheric laminar premixed flames of C_2-fuels: ethane, ethylene and acetylene. The value of the critical equivalence ratio, ϕ_c, for a given fuel and a given maximum flame temperature, T_m, was determined by computing flames with different equivalence ratios. The maximum flame temperature in these runs was maintained approximately the same by adjusting, similarly to the experiment, the amount of N_2 in the mixture. For each of the fuels, at least two series of flames were simulated, each at a different maximum flame temperature, in order to test the temperature dependence predicted for ϕ_c.

The numerical simulation of soot particle formation was performed in two stages: first, the production of the initial PAH species; and second, PAH further growth and nucleation and growth of soot particles. In the first stage, PAH formation up to coronene was simulated in a burner-stabilized flame configuration with a specified temperature profile and flow rate. The maximum temperature reached in the free-flame simulation, with a given ϕ, was matched to the corresponding experimental value measured by Harris et al.[2] The adjustment of the maximum flame temperature was accomplished, similarly to the experiment, by varying the amount of N_2 present in the mixture, but not necessarily equal to the experimental level of dilution, and being typically 5% higher in N_2 mole fraction. In the second stage, the profiles of H, H_2, C_2H_2, O_2, OH, H_2O and acepyrene (A_4R5) obtained in the flame simulation were used as input for the simulation of the growth of PAHs beyond acepyrene by the technique of chemical lumping and the soot particle nucleation and growth by a method of moments.

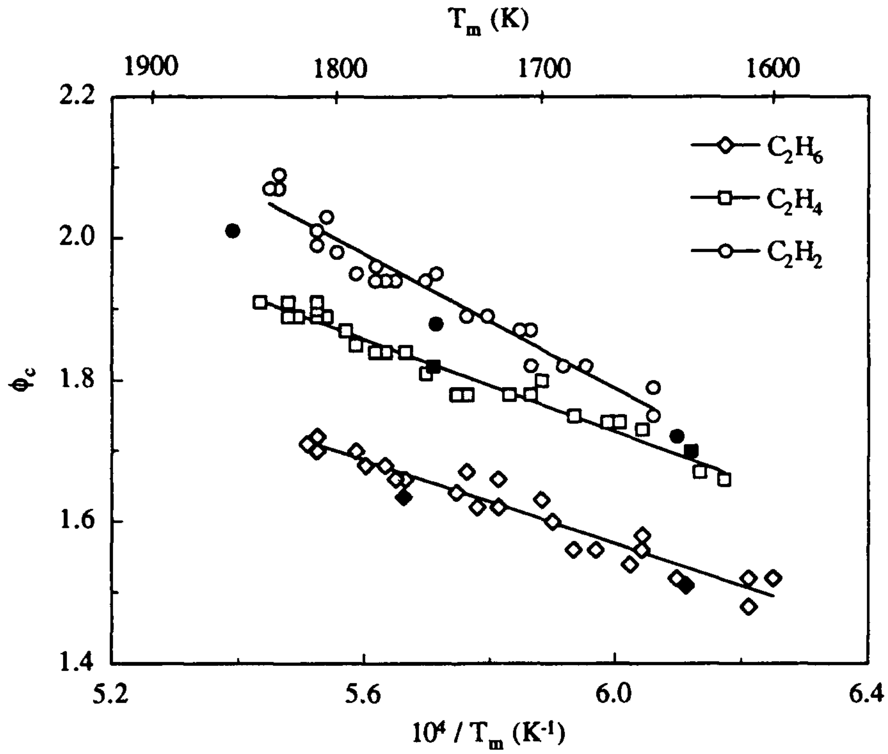

Figure 1. Comparison of the computed and experimentally determined critical equivalence ratios ϕ_c for ethane, ethylene and acetylene flames, as a function of the maximum flame temperature T_m. The open symbols represent the experimental data of Harris et al.,[2] solid lines—linear fits to the experimental points, and solid symbols—the present computational predictions.

The critical equivalence ratios determined in this manner for the three fuels are displayed in Fig. 1, where they are compared with the experimental data of Harris et al.[2] As can be seen in this figure, the computed critical equivalence ratios follow the correct temperature dependence for each fuel, i.e., the critical equivalence ratio increases as the flame temperature increases, and the correct dependence on fuel type, for a constant flame temperature T_m, i.e., acetylene soots earlier than ethylene which soots earlier than ethane. The quantitative agreement between the computed and experimental values of ϕ_c is also reasonable, considering the lack of the precise experimental data for model input and boundary conditions, uncertainties in the model parameters, and the fact that the reaction mechanism was adopted from the previous study[3] without any adjustments.

The analysis of the computational results strongly suggested that the appearance of soot and hence the sooting limits in these flames is controlled by two factors: concentration of acetylene and the growth of PAHs. The second factor—the PAH build-up—is limited by the rise in flame temperature towards the end of the main reaction zone. The oxidation of PAHs, the molecular precursors to soot particles, was not found to be a controlling factor. This does not mean, however, that hydrocarbon oxidation does not play a role in soot formation. On the contrary, oxidation of pre-aromatic-ring species, like C_2H_3 by O_2, determines to a great degree the concentration level of phenyl, the first aromatic ring. Also, the oxidation of PAHs by OH begins to be more pronounced in locations away from the main flame zone, where OH becomes the dominant oxidant.

Evaluation of the Enthalpies of Formation of PAH Molecules and Radicals[4]

As part of the ongoing efforts on soot formation model development and refinement, the enthalpies of formation of polycyclic aromatic hydrocarbon (PAH) molecules, radicals and substituted aromatics were investigated. The enthalpy data used in previous and current modeling efforts have been mainly derived from Benson's group additivity method. Recent results from ab initio quantum mechanical calculations have shown that for large peri-condensed PAHs, the enthalpies of formation predicted by the group additivity method could be off by as much as 10 kcal/mol.[5] The objective of our work was to determine accurately the enthalpies of formation for the major aromatic species involved in the growth of PAHs and soot in high-temperature environments. These species include PAH molecules up to 3-circumcoronene, PAH radicals up to coronyl, and some substituted aromatics.

A method for accurate and economical estimation of the enthalpies of formation for benzenoid aromatic species was developed which combines semiempirical quantum-mechanical calculations with group corrections. In this method, the deviation between experimental and calculated enthalpies of formation is partitioned into structural groups. The general idea is to use a calculation method which is computationally less demanding than quantum ab initio but physically more realistic than group-additivity calculations, and then to correct the results using a group-additivity scheme for the numerical inaccuracy of the semiempirical quantum-chemical method. The advantage of this approach is that it can be applied consistently to both molecules and radicals. The obtained with this method standard-state enthalpies of formation compare well with the experimental data and with the results of ab initio quantum-mechanical calculations available in the literature. The calculated enthalpies of formation for large peri-condensed aromatic molecules are extended smoothly to the limit of a graphite monolayer.

The developed method was also applied to examine the stability of aryl radicals as functions of molecular size and radical position, which indicates that the strength of aryl–H bond is essentially independent of molecular size, but dependent on the neighboring geometry of the C–H bonds. Smaller aryl–H bond strengths are predicted for the C–H bonds situated in the bay region of the aromatic molecules and are the results of larger steric repulsion between the neighboring H atoms.

Transport Properties of Polycyclic Aromatic Hydrocarbons[6]

Diffusion of gaseous PAHs is an important process that significantly affects the results of numerical simulations of soot formation in hydrocarbon flames. Although several empirical correlations are available for estimation of diffusion coefficients of aromatic compounds, they are not easy to implement in the computer codes now in use by the combustion community. The common practice is to compute transport properties, including diffusion coefficients, through the parameters of Lennard-Jones 12-6 (LJ) potential, and hence the LJ collision diameters σ and potential energy well depths ε, specified for individual chemical compounds, serve as input to flame codes. Such approach assures not only consistency among various transport properties, such as gaseous viscosities and thermal conductivities, but also consistency in evaluation of transport properties with calculations of reaction rates, such as those encountered in coagulation of PAH species.

A method was developed for systematic evaluation of the Lennard-Jones parameters for PAH compounds, in which correlations for these parameters are derived using a group contribution technique for critical temperatures and pressures and the Tee-Gotoh-Stewart correlations of corresponding states. The Lennard-Jones self-collision diameters and well depths of 29 polycyclic aromatic hydrocarbons were estimated using this approach and are shown to correlate with the molecular weights of aromatics. The correlation obtained for the self-collision diameters exhibits the one-third power in the molecular weight, indicating that, due to rotation, planar gaseous PAH molecules behave like spherical particles. The gaseous binary diffusion coefficients of aromatics in common gases were calculated with Chapman-Enskog equation using the estimated Lennard-Jones parameters and were found to compare well with the available experimental data and the predictions of one of the most reliable empirical approximations.

Semiempirical Quantum-Mechanical and RRKM Studies[7] *of Reaction* $C_8H_7^+ + C_2H_2 \rightarrow C_{10}H_9^+$

The title reaction is one of the key steps in the mechanism proposed by Calcote and coworkers.[8] Seven major isomers for the $C_{10}H_9^+$ adduct and 11 possible product channels were identified in our study, indicating the complexity of the reaction. The energetics and molecular parameters of the reactants, intermediate species, products, and transition states were evaluated using the semiempirical quantum-mechanical AM1 method. The rate coefficients and their pressure and temperature dependence were then calculated using the RRKM theory with a full consideration of angular momentum conservation. The microscopic rate coefficients for the reaction channels involving the dissociation of the energized complexes were determined with the microcanonical variational transition state theory. The calculations were performed for a temperature range of 300–2000 K and pressures of 20 and 760 torr. These physical conditions correspond to experimental studies of ion formation in flames.[9,10]

The major results of this study can be summarized as follows. At temperatures below 1000 K, the overall rate coefficient is equal to that of the Langevin limit, 6×10^{14} $cm^3mol^{-1}s^{-1}$.

However, at flame temperatures above 1500 K, where most of the ions are observed in laminar premixed flames, the rate coefficients of the reactions between PAH ions and acetylene could be as much as three orders of magnitude lower than the Langevin limit. The main reason for this is insufficient collisional stabilization. Thus, it is expected that many, if not all, aryl ion-molecule reactions occurring in hydrocarbon flames may have rate coefficients on the same order of magnitude as those of neutral aryl radical-acetylene reactions. The latter are typically on the order of 10^{12} $cm^3mol^{-1}s^{-1}$. This result suggests that the rate coefficients used in the reaction model of ion formation proposed by Ca'cote and coworkers[8] may be several orders of magnitude too high.

Pressure Effect on Soot Formation

The ability to predict soot formation at high pressures is of considerable interest because most practical combustion devices operate at elevated pressures. Yet, most laboratory flame experiments focusing on soot were performed at subatmospheric and atmospheric conditions. Recently, a systematic investigation of pressure effect on soot formation in laminar premixed flames of ethylene have been undertaken by Jander, Wagner and coworkers.[11-14] In their studies, the pressure was varied from 1 to 100 bar. The objective of the present study was to test whether our recently developed soot formation model[3,15] is able to account for these observations. Specifically, we chose to simulate the 10 bar flames of Bönig et al.[13] To determine the effect of pressure on soot production, the simulation results were compared to those obtained for an atmospheric flame.

The computational model consists of the following principal processes:[3,15] initial aromatic ring formation during small hydrocarbon pyrolysis and oxidation, planar PAH growth through the hydrogen-abstraction–acetylene-addition (HACA) reaction mechanism, particle nucleation through coalescence of PAHs into three-dimensional clusters, particle growth by coagulation and surface reactions of the forming clusters and particles.

A recently updated 500-reaction and 100-species mechanism was used to describe the initial hydrocarbon pyrolysis and oxidation, and PAH formation and growth up to coronene. The formation of the first aromatic ring proceeds via the reactions

$$C_3H_3 + C_3H_3 \rightarrow \text{benzene} \quad (1)$$

$$n\text{-}C_4H_3 + C_2H_2 \rightarrow \text{phenyl} \quad (2)$$

$$\ell\text{-}C_6H_4 + H \rightarrow \text{phenyl} \quad (3)$$

$$n\text{-}C_6H_5 \rightarrow \text{phenyl} \quad (4)$$

$$n\text{-}C_4H_5 + C_2H_2 \rightarrow \text{benzene} + H \quad (5)$$

$$\ell\text{-}C_6H_6 + H \rightarrow \text{benzene} + H \quad (6)$$

$$n\text{-}C_6H_7 \rightarrow \text{benzene} + H \quad (7)$$

The rate coefficient of reaction (1) was assigned a value of 1×10^{11} $cm^3mol^{-1}s^{-1}$, based on an analysis of benzene formation in subatmospheric and atmospheric-pressure flames. The rate coefficients of reactions (2) – (7) were calculated using the RRKM theory.[16]

Flame simulations were carried out using the Sandia burner code.[17] The transport properties of PAHs were taken from our recent evaluation.[6] The computed profiles of H, H_2, C_2H_2, O_2, OH, H_2O and the rate of pyrene formation were then used as inputs for the simulation of PAH growth beyond pyrene and of soot formation. The PAH growth beyond pyrene was described by a replicating HACA reaction sequence given in Table 1. The rate coefficients of the replicating reactions listed in Table 1 were estimated based on analogous reactions of one- to three-ring aromatics. The formation of soot particles was assumed to be initiated by the coalescence of two PAH molecules. The subsequent growth of soot particles proceeds through particle-particle and particle-PAH coagulation and through surface reactions. Particle coagulation was assumed to be in the free-molecular regime, with a size-independent enhancement factor of 2.2.[22] Modeling of PAH growth beyond pyrene and of soot particle dynamics was accomplished using the method of moments.[15]

In the present model, the surface growth is assumed[3,15] to occur due to reactions of surface radicals with C_2H_2. The surface oxidation is assumed to occur via reactions of surface radicals with O_2 and of the particle surface with OH. The surface reactions and their associated rate coefficients are provided in Table 2. The rate coefficients of the heterogeneous reactions, S1–S4, were estimated based on analogous gas-phase reactions of one-ring aromatics. The mechanism of soot particle oxidation by OH is not well understood and therefore it was described by the probability of reaction when an OH radical collides with the particle surface. This probability was taken to be 0.13 from the work of Neoh et al.[23]

The rates of the surface reactions, S1–S4, for the ith particle were described by[3,15]

$$k_S\, C_g\, \alpha\, \chi_S\, S_i\, N_i, \tag{8}$$

where k_S is the per-site rate coefficient, C_g is the concentration of gaseous species g, α is the fraction of surface sites available for reaction, whose value will be discussed below, χ_S is the number density of surface sites, and S_i and N_i are the surface area and number density of the ith particle, respectively.

Three 10 bar, burner-stabilized, ethylene-air flames were selected for the simulation. To examine the influence of pressure on soot production, an 1 bar, burner-stabilized flame was also considered. The flame conditions are summarized in Table 3. The following experimental data were supplied by Jander:[24] temperatures measured at different distances from the burner surface for Flames 1 – 4, soot volume fraction profiles in Flames 2 – 4, and in Flame 1, the mole fractions of major flame products and PAH species at a distance of 3 cm from the burner surface.

The principal difficulty in the simulation of these 10-bar flames is that the temperature profile in the main-reaction zone is unknown. In all cases, measurements were made only in the post-flame zone,[24] therefore the temperature profile in the main-reaction zone had to be extrapolated from the post-flame measurements. For Flames 1 – 3, the distance between the burner surface and the first measured temperature point is 4 to 5 times the width of the main-reaction zone with the post-flame temperature profile exhibiting a marked curvature (Fig. 1a). These factors make the reliable temperature extrapolation difficult. It was therefore necessary to impose additional constraints in order to obtain the entire temperature profile required for the

TABLE 1. Replicating reaction mechanism of PAH growth beyond pyrene

No.	Reaction[a]	$k = AT^n e^{-E/RT}$: A ($cm^3 mol^{-1} s^{-1}$)	n	E ($kJ\ mol^{-1}$)	Comments
L1	$A_{i-1}\cdot + C_2H_2 \rightarrow A_i + H$	6.6 (33)	−5.92	94.5	1 atm, *b*
		1.2 (33)	−5.59	106.9	10 atm, *b*
L1a	$A_i + H \rightleftharpoons A_i\cdot + H_2$	2.5(14)		66.9	*c*
L1b	$A_i + OH \rightleftharpoons A_i\cdot + H_2O$	2.1(13)		19.1	*d*
L1c	$A_i\cdot + H \rightleftharpoons A_i$	6.4 (20)	−2.15	7.9	1 atm, *e*
		2.2 (26)	−3.67	24.6	10 atm, *e*
L1d	$A_i\cdot + O_2 \rightarrow$ products	2.0(12)		31.3	*f*
L2	$A_i\cdot + C_2H_2 \rightleftharpoons A_iC_2H + H$	5.1 (38)	−7.09	123.7	1 atm, *b*
		2.8 (34)	−5.81	132.3	10 atm, *b*
L2a	$A_iC_2H + H \rightleftharpoons A_iC_2H\cdot + H_2$	2.5(14)		66.9	*c*
L2b	$A_iC_2H + OH \rightleftharpoons A_iC_2H\cdot + H_2O$	2.1(13)		19.1	*d*
L2c	$A_iC_2H\cdot + H \rightleftharpoons A_iC_2H$	6.4 (20)	−2.15	7.9	1 atm, *e*
		2.2 (26)	−3.67	24.6	10 atm, *e*
L2d	$A_iC_2H\cdot + O_2 \rightarrow$ products	2.0(12)		31.3	*f*
L3	$A_iC_2H\cdot + C_2H_2 \rightleftharpoons A_{i+1}\cdot$	1.4 (52)	−11.58	108.9	1 atm, *b*
		1.1 (44)	−9.08	97.9	10 atm, *b*
L3a	$A_{i+1} + H \rightleftharpoons A_{i+1}\cdot + H_2$	2.5(14)		66.9	*c*
L3b	$A_{i+1} + OH \rightleftharpoons A_{i+1}\cdot + H_2O$	2.1(13)		19.1	*d*
L3c	$A_{i+1}\cdot + H \rightleftharpoons A_{i+1}$	6.4 (20)	−2.15	7.9	1 atm, *e*
		2.2 (26)	−3.67	24.6	10 atm, *e*
L3d	$A_{i+1}\cdot + O_2 \rightarrow A_i$ + products	2.0(12)		31.3	*f*
L4	$A_{i+1}\cdot + C_2H_2 \rightleftharpoons A_{i+2} + H$	6.6 (33)	−5.92	94.5	1 atm, *b*
		1.2 (33)	−5.59	106.9	10 atm, *b*
L4a	$A_{i+2} + H \rightleftharpoons A_{i+2}\cdot + H_2$	2.5(14)		66.9	*c*
L4b	$A_{i+2} + OH \rightleftharpoons A_{i+2}\cdot + H_2O$	2.1(13)		19.1	*d*
L4c	$A_{i+2}\cdot + H \rightleftharpoons A_{i+2}$	6.4 (20)	−2.15	7.9	1 atm, *e*
		2.2 (26)	−3.67	24.6	10 atm, *e*
L4d	$A_{i+2}\cdot + O_2 \rightarrow A_{i+1}$+ products	2.0(12)		31.3	*f*
L5	$A_{i+2}\cdot + C_2H_2 \rightarrow A_i + H$	6.6 (33)	−5.92	94.5	1 atm, *b*
		1.2 (33)	−5.59	106.9	10 atm, *b*

[a] The rate coefficients for the reverse directions were determined via equilibrium constants. [b] Based on RRKM calculations for one- to three-ring aryl reaction with acetylene.[16] [c] Taken from Kiefer et al.[18] for the analogous reaction of benzene. [d] Taken from Madronich and Felder[19] for the analogous reaction of benzene. [e] Based on RRKM calculations for the phenyl and hydrogen atom association reaction with parameters taken from Rao and Skinner.[20] [f] Taken from Lin and Lin[21] for the analogous reaction of phenyl.

TABLE 2. Reaction mechanism of soot particle surface growth and oxidation

No.	Reaction[a]			$k = AT^n e^{-E/RT}$		
				A (cm^3s^{-1})	n	E ($kJ\ mol^{-1}$)
S1	C_{soot}–H + H	→	C_{soot}• + H_2	4.2 (−10)		66.9
S−1	C_{soot}• + H_2	→	C_{soot}–H + H	6.5 (−12)		39.0
S2	C_{soot}• + H	→	C_{soot}–H	1.7 (−10)		
S3	C_{soot}• + C_2H_2	→	C_{soot}–H + H	1.4 (−12)	0.4	35.1
S4	C_{soot}• + O_2	→	products	3.7 (−12)		31.3
S5	C_{soot}–H + OH	→	products	0.13[b]		

[a] C_{soot}–H represents an arm-chair site on the soot particle surface and C_{soot}• the corresponding radical.
[b] Reaction probability upon OH collision with soot particle surface.[23]

TABLE 3. Conditions of simulated burner-stabilized ethylene-air flames[24]

Flame no.	Pressure (bar)	C/O	Cold gas velocity (cm/s)	Maximum flame temperature (K)
1	10	0.68	6.0	1880[a]
2	10	0.673	3.0	1895[a]
3	10	0.60	6.0	2017[a]
4	1	0.69	5.9	1711[b]

[a] Equal to the adiabatic flame temperature. [b] Obtained by extrapolating the post-flame temperature data and assuming the maximum flame temperature is located near the point where the first soot volume fraction measurement is reported.

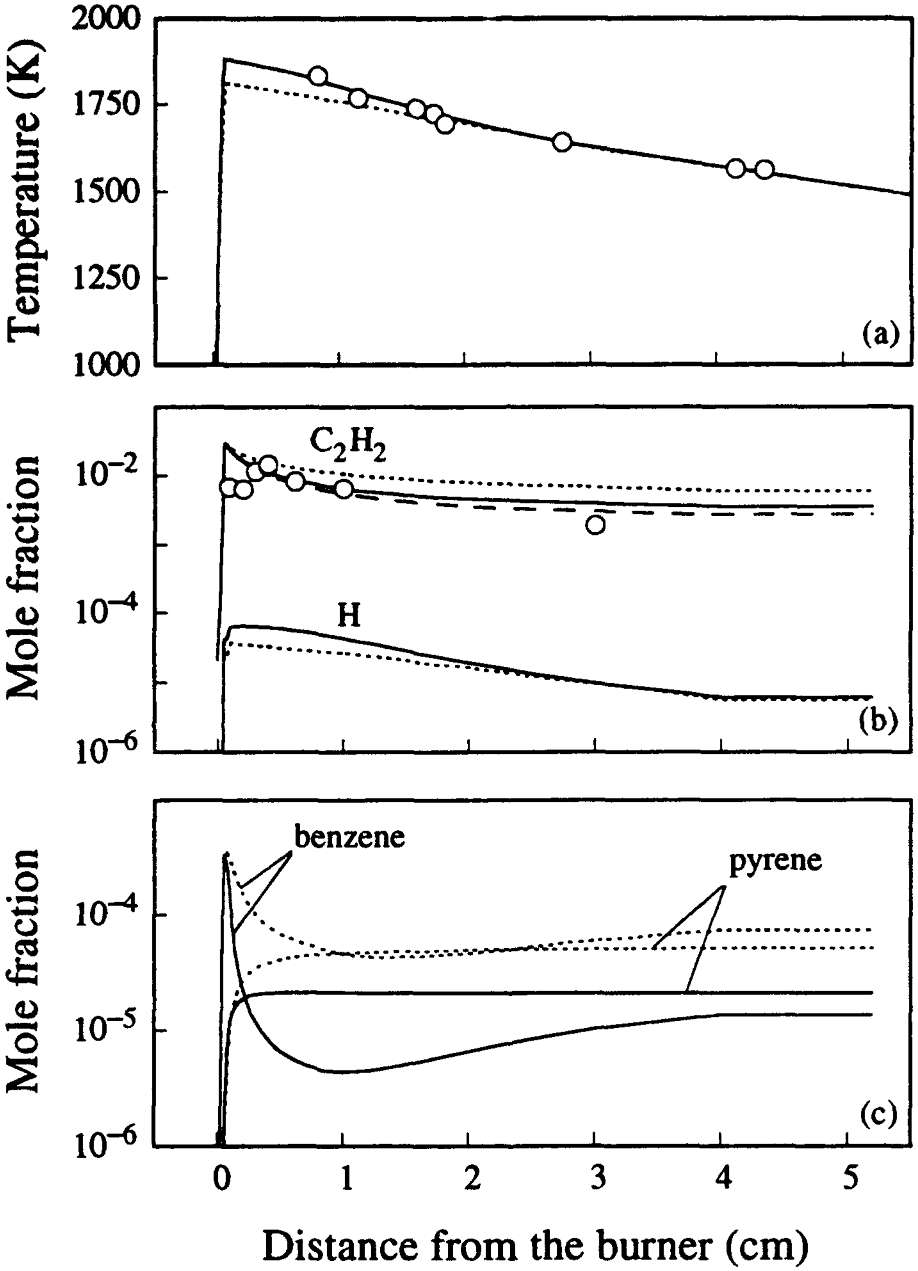

Figure 1. Flame 1. (a) lines—assumed temperature profiles: solid line—the location of T_{max} is at the onset of soot luminosity, $T_{max} = T_{ad}$; dotted line—$T_{max} = T_{ad} - 70$ K. (b) and (c) concentrations of species indicated, computed with temperature profiles shown in (a); dashed line in (b)—with consumption of acetylene by soot surface reaction. Symbols in (a) and (b) are experimental data.[24]

simulations. It was assumed that (1) the flame temperature reaches maximum at the location where the soot luminosity is first seen: 0.1 cm above the burner for Flames 1 and 3 and 0.2 cm for Flame 2, and (2) the maximum flame temperature, T_{max}, is equal to the adiabatic flame temperature, T_{ad}.

Unlike Flames 1 – 3, temperature extrapolation can be made with a greater confidence for the atmospheric-pressure flame, Flame 4. In this flame, measurements were made relatively close to the main-reaction zone. In addition, the post-flame temperature profile is nearly linear. Therefore, T_{max} was determined by extrapolating the temperature data to the position where the first soot volume fraction measurement was reported, *i.e.*, 0.3 cm from the burner surface. The maximum temperature of Flame 4 determined in this manner is about 200 K lower than T_{ad}.

An example of the temperature extrapolation for a 10-bar flame is shown in Fig. 1a. The solid lines in all panels of Fig. 1 were obtained with the assumption that $T_{max} = T_{ad}$. A sensitivity test was performed by assuming $T_{max} = T_{ad} - 70$ K, which is shown by the dotted line in Fig. 1a. The mole fractions of H, C_2H_2, benzene and pyrene computed using the two temperature profiles are presented in Figs. 1b and 1c. The differences in the H and C_2H_2 concentrations calculated with the two temperature cases are insignificant. For benzene and pyrene, the post-flame profiles are clearly affected by the assumption made on T_{max}. However, the most important properties for the nucleation of soot particles—the initial part of the concentration profiles and their peak values—are essentially unaffected by this assumption. The computational features observed above are the same for all of the flames considered.

In Fig 1b, a comparison of the model prediction and the experimental data for acetylene in Flame 1 is presented. It is apparent that the experimental data are well predicted by the model. The agreement is particularly good in the region where soot gains most of its mass through acetylene surface reactions, *i.e.*, between 0.2 to 1 cm from the burner surface. The seeming over-prediction of the acetylene peak mole fraction is not caused by the assumption made on T_{max}, as the maximum mole fractions of acetylene computed using the two temperature profiles shown in Fig. 1a are essentially the same. As shown in Fig. 1b, the acetylene concentration at 3 cm from the burner surface was more closely predicted with the assumption $T_{max} = T_{ad}$ than using lower values of T_{max}. As will be discussed later, acetylene consumption by soot was found to be insignificant over the entire flame.

The kinetic model predicted reasonably well other measured species concentrations, see Fig. 2. The computed main-reaction zone width is about 0.1 cm, which is consistent with the assumed distance between the burner surface and the location of the maximum flame temperature. The experimental concentrations of H_2, H_2O and CO_2 at 3 cm from the burner surface were fairly well reproduced by the model, with the exception of CO which was slightly over predicted. Such a level of agreement is typical, and commonly seen for even better studied, better spatially resolved sub-atmospheric flames (see, *e.g.*, Ref. 25).

As shown in Figs. 2c and 2d, the PAH concentrations at 3 cm from the burner surface were computed within a factor of 2 to 3 of the experimental values. For this flame, the measured post-flame concentrations of naphthalene were larger than those of benzene. This was successfully predicted by the model. Analysis of reaction pathways indicated that for Flames 1 – 3, benzene is produced through reactions 5 – 7 with approximately equal rates. With the present assignment for the rate coefficient of reaction 1, the contribution of propargyl recombination to benzene production is negligible.

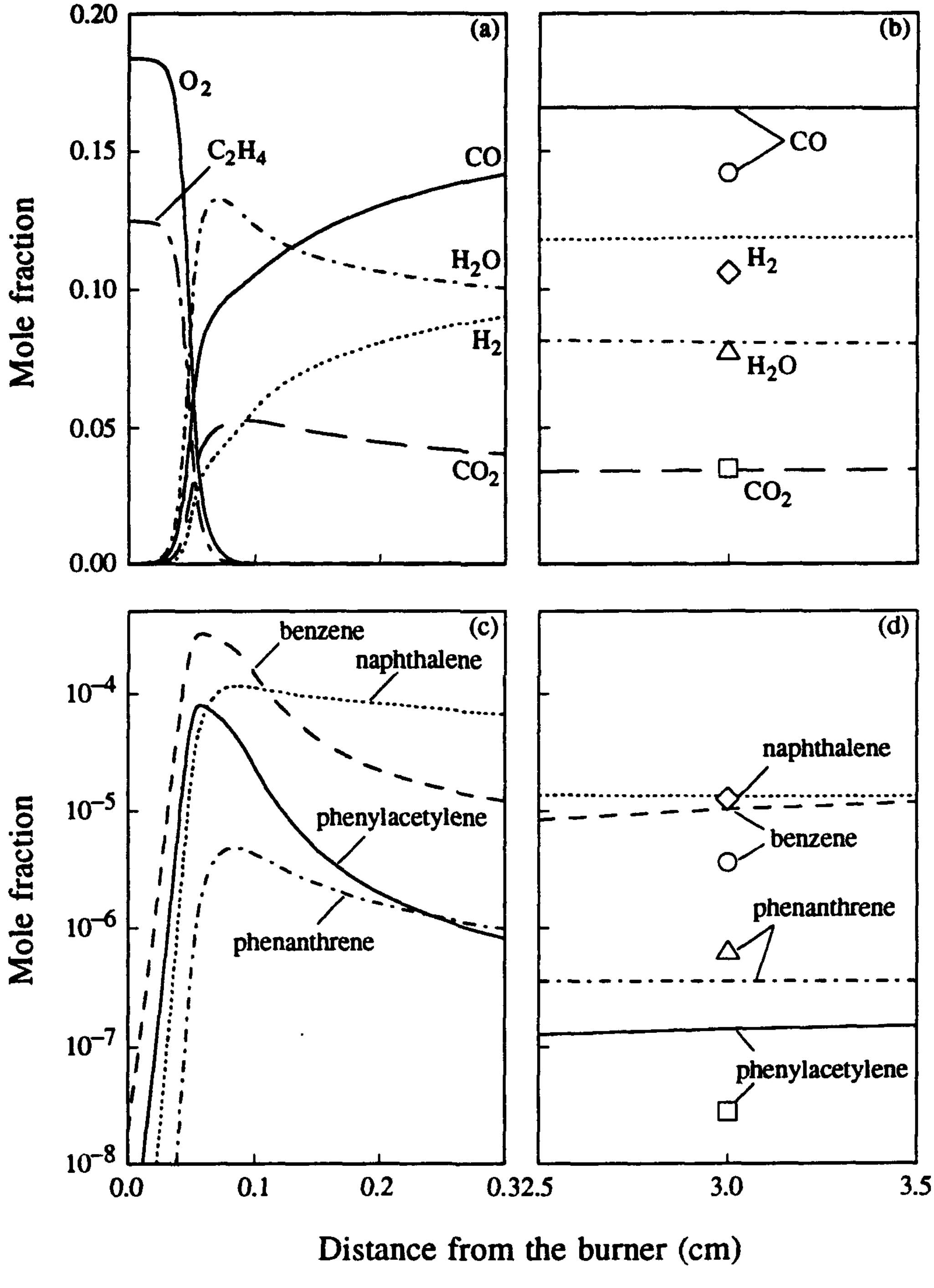

Figure 2. Computed (lines) and experimental[24] (symbols) concentrations of selected species for Flame 1.

A characteristic behavior of ethylene flames is the production of large amounts of vinyl radicals in the preflame zone. The vinyl radicals react quickly with ethylene to produce 1,3-butadiene (C_4H_6) through $C_2H_4 + C_2H_3 \rightarrow C_4H_6 + H$. 1,3-butadien-1-yl ($n$-$C_4H_5$) is then produced from C_4H_6 through H-abstraction by OH. The further reaction of C_4H_6 with C_2H_3 leads to 1,3,5-hexatriene (ℓ-C_6H_8). 1,3,5-hexatrien-1-yl (n-C_6H_7) is produced from ℓ-C_6H_8 by the H-abstraction reactions. At the same time, vinyl radicals decompose to acetylene via the reaction $C_2H_3 \rightarrow C_2H_2 + H$. The addition of vinyl to acetylene produces vinylacetylene (C_4H_4), which in turn reacts with C_2H_3 to produce 1,3-hexadien-5-yne (ℓ-C_6H_6). These reaction pathways are very similar to those identified for near-sooting-limit atmospheric flames of ethylene.[1]

The comparison of the computed and experimental profiles of soot volume fractions are presented in Fig. 3 for Flames 2 and 3, and Fig. 4a for Flames 1 and 4. Inspection of these figures indicates that the shape of the experimental soot profiles for all of the flames is well predicted by the model. The quantitative agreement was obtained by adjusting a single parameter—the fraction of soot surface sites available for reaction, α in Eq. (8).

Parameter α was introduced[3] to represent a steric factor, whose value should decrease with the increase in flame temperature. This is because at high temperatures, soot particle structural units are expected to be more mobile and align themselves in a more concentric manner, so that the access of gaseous species to the reactive carbon sites is limited. Figure 5 displays the values of α obtained in the present and past[15] studies. It is observed that α markedly decreases as the maximum flame temperature increases. Sensitivity runs indicated that the numerical predictions for soot volume fraction are extremely sensitive to the assumed value of α. As shown in Fig. 3a for Flame 2, a factor of 10 difference in α causes the soot volume fraction to differ by more than a factor of 30. The latter change in soot volume fraction is expected to be larger than the uncertainties of both the experiment and the model. In addition, the absolute values obtained for α lie in a reasonable range. Thus, it is likely that the trend shown in Fig. 5 reflects the dependence of α on flame temperature. At the same time, no clear pressure dependence of α is observed in Fig. 5.

An important feature of the present study is that the experimentally observed effect of pressure on soot volume fraction is well accounted for by the model (Fig. 4a). Experimentally, Bönig et al.[13] determined in ethylene-air flames that the final soot volume fraction, $f_{v\infty}$, is proportional to P^2 for $P \leq 10$ bar. Above 10 bar, the dependence of soot production on pressure weakens and $f_{v\infty}$ is proportional to P.[14] It was suggested[14] that the weakening pressure dependence is due to the increasing acetylene consumption by soot surface reactions, thus depleting the principal surface growth species. While simulations over a broader range of pressure were not attempted in the present study, the influence of pressure on soot production is examined by concentrating on the comparison between Flame 1 at 10 bar and Flame 4 at 1 bar.

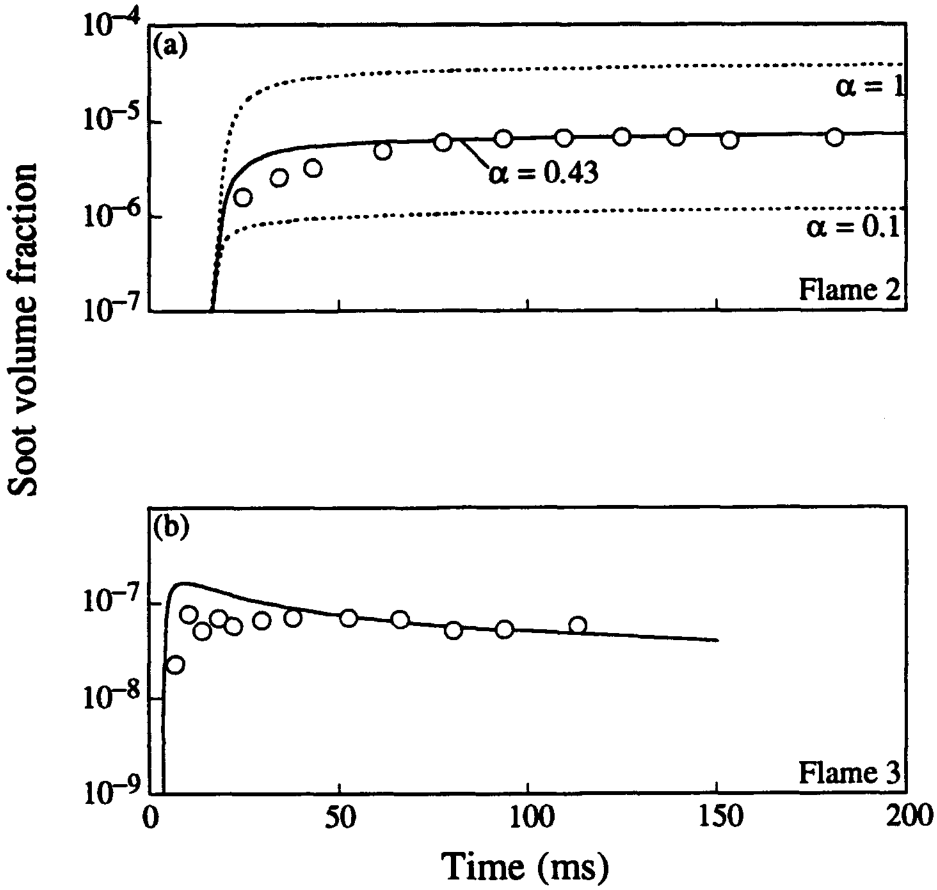

Figure 3. Comparison of model predictions and experimental data[24] for soot volume fraction in Flames 2 and 3.

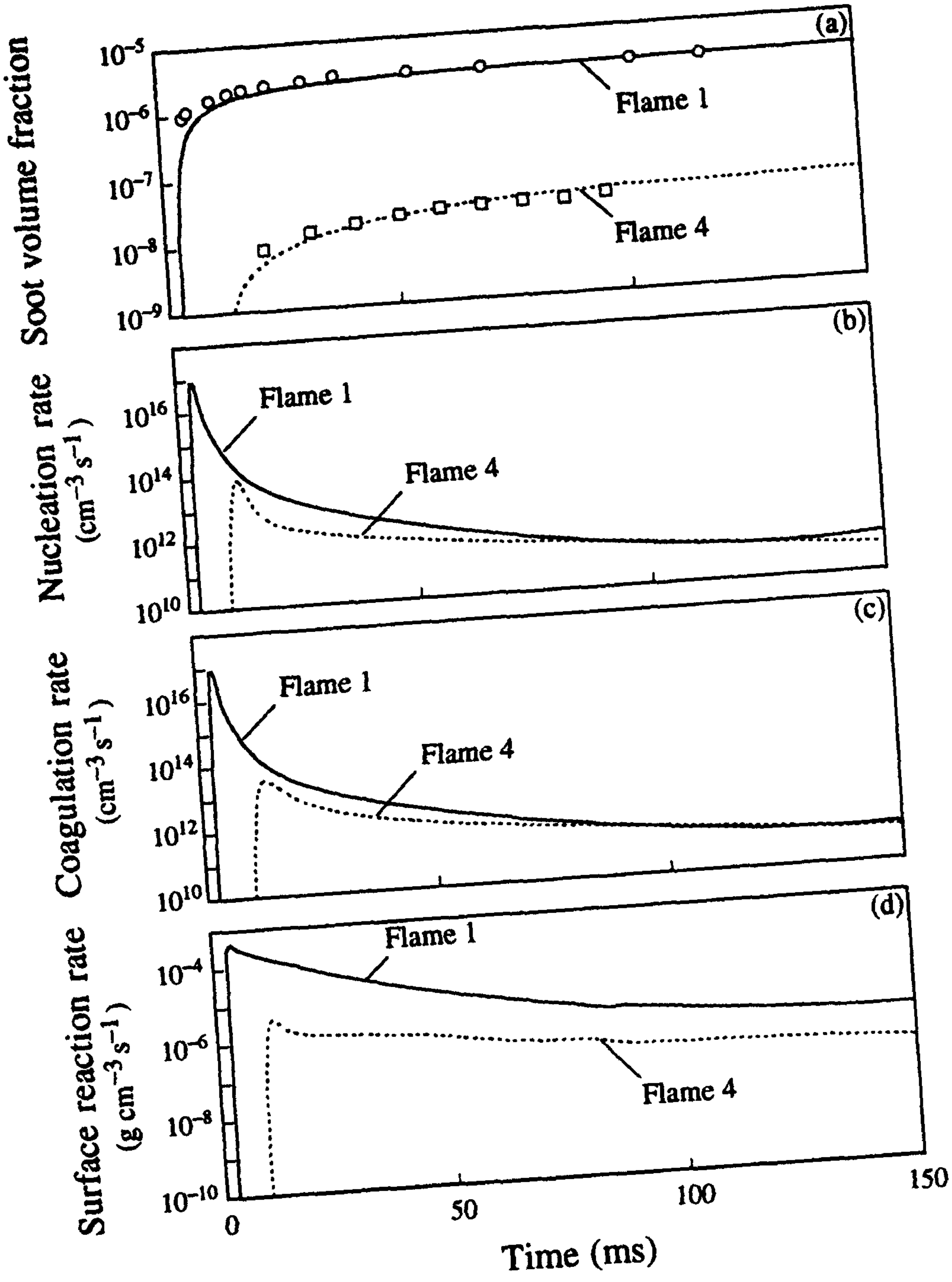

Figure 4. Comparison of Flames 1 and 4. Lines are model predictions; symbols—experimental results: squares—from Ref. 24, circles—obtained by interpolation between two similar flames with C/O equal to 0.672 and 0.696.[24]

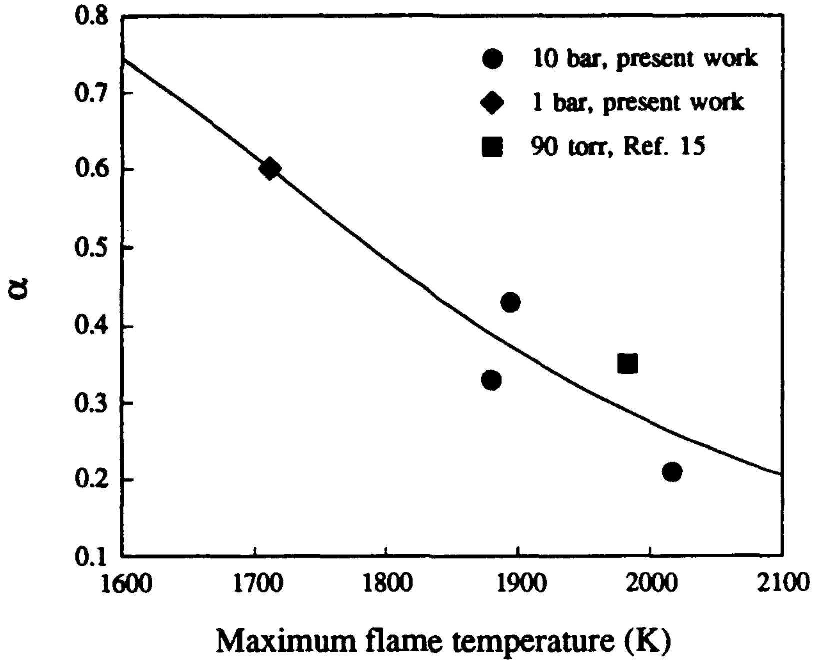

Figure 5. The fraction of soot surface radical sites available for reaction, α, plotted as a function of maximum flame temperature, T_{max}. The line is a fit to the data, $\alpha = [\tanh(8168/T_{max} - 4.57)+1]/2$.

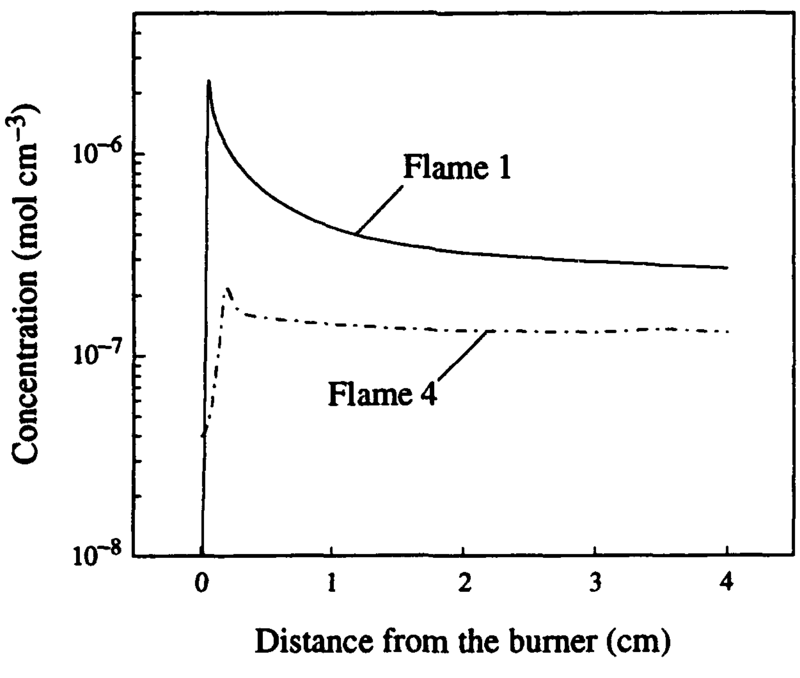

Figure 6. Comparison of the acetylene concentrations computed for Flames 1 and 4.

First, the degree of acetylene consumption was examined for Flame 1. A series of iterative flame simulations was performed. Each iteration included the consumption of acetylene by its surface reaction with soot particle and used the particle surface area obtained from the previous iteration. The final, converged result for the acetylene concentration is shown in Fig. 1b. A comparison with the original profile indicates that an observable amount of acetylene is indeed consumed by soot. However, the decrease in the acetylene concentration is quite small and has little effect on the computed soot volume fraction under the conditions of Flame 1. The deviation between the experimentally determined post-flame concentrations of acetylene and the computed concentrations is significantly smaller than that obtained by Böhm et al.[14]

To understand the factors governing the observed pressure dependence of soot production, the rates of nucleation, coagulation and surface growth of the soot particles were examined. Inspection of Fig. 4b indicates that the peak nucleation rate of soot in Flame 1 is about three orders of magnitude higher than the peak rate in Flame 4. This is caused by larger concentrations of PAHs produced in Flame 1. The nucleation is balanced by coagulation for both flames. The resulting peak number density of soot particles in Flame 1 is about a factor of 50 larger than the peak value in Flame 4. Due to the large coagulation rate, the soot number density in Flame 1 decreases quickly, approaching the value for Flame 4 after ~20 ms of reaction time. During this same reaction period, the soot volume fraction increases rapidly due to the surface growth reactions, and nearly reaches its final value by the end of the reaction period. Thus, soot gains most of its mass during the same period of intense coagulation.

The rates of surface growth differ in Flames 1 and 4 by approximately two orders of magnitude during the initial reaction times when soot gains most of its mass. Since surface growth provides the ultimate soot mass, the quantitative difference in $f_{v\infty}$ between Flames 1 and 4 is caused by the 10^2 difference in the surface growth rates. The soot surface growth under the conditions of the simulated flames is predominantly due to the reactions of acetylene with the soot particle surface. The surface growth rate is thus proportional to the acetylene concentration. In the region where soot gains most of its mass, the absolute concentrations of acetylene in Flames 1 and 4 differ, due to the pressure difference, by only one order of magnitude (Fig. 6). Thus, the difference in the acetylene concentration alone cannot fully explain why the surface growth rate in Flame 1 is two orders of magnitude higher than that in Flame 4.

Soot surface area is an additional factor contributing to the growth rate. The surface area is determined not only by surface growth, but also by nucleation and coagulation. An additional test was performed to determine the contribution of nucleation to $f_{v\infty}$. In this test, the peak nucleation rate of Flame 1 was artificially reduced to 10^{14} $cm^{-3}s^{-1}$, *i.e.*, equal to that of Flame 4. The resulting $f_{v\infty}$ was lowered by about an order of magnitude. Thus, the larger nucleation rate and the higher acetylene concentration contribute about equally to the increased value of $f_{v\infty}$ in Flame 1. The above analysis suggests that for soot formation under the conditions simulated nucleation is as critical as surface growth.

As described earlier, the present model assumes that the nucleation of soot particles is initiated by PAH coalescence. Consequently, the nucleation rate depends strongly on PAH concentrations. Inspection of the computed results indicates that the influence of pressure on the total concentration, particularly on the concentration of acetylene, has the strongest effect on the production of PAHs and hence on the nucleation of soot particles.

A secondary effect of pressure on the production of PAHs arises from the pressure dependence of reaction rate coefficients. This pressure effect arises from the reactions whose energized adducts undergo collisional stabilization. A test run under the conditions of Flame 1, but with the pressure-dependent rate coefficients set equal to those at 1 bar, results in the peak concentration of naphthalene that is a factor of 4 lower than that computed with the rate coefficients at 10 bar.

It is thus demonstrated that the detailed chemical kinetic model of soot formation, developed and tested earlier for subatmospheric and atmospheric flames, can quantitatively reproduce the experimental soot volume fraction profiles collected in a number of 10 bar, burner-stabilized, ethylene-air flames. Analysis of the computational results suggests that the consumption of acetylene by soot particle surface growth is insignificant up to 10 bar. In addition, the influence of pressure on soot production arises mainly from a larger concentration of acetylene at high pressure, which affects both the soot surface growth and the nucleation of soot particles.

Reduced Model for PAH and Soot Formation

The entire reaction mechanism—from the initial hydrocarbon to soot particles—can be divided into three parts, each reduced with a different method: small-molecule reactions describing the main combustion environment and the formation of the first aromatic ring; its growth to pyrene; and nucleation, growth and oxidation of soot particles. The former part, small-molecule chemistry, is a subject of continuous efforts of the research community; and the latter, particle dynamics, has been addressed by us previously using the method of moments. Here, a reduced model for PAH formation and growth, the central part of the soot-precursor chemistry, is presented.

A reaction sequence leading from benzene to pyrene, adopted for the present study, is shown in Fig. 7. This reaction scheme is based on both our past results[1,3,15] and a reaction flux analysis performed in the present study using an extensive reaction set under the conditions typical of high-pressure turbulent combustion. The nomenclature for chemical species used in Fig. 7 and throughout the manuscript has been introduced previously.[26] Briefly, A_i represents a species composed of i fused aromatic rings; e.g., A_1 is benzene and A_4 pyrene. A_iC_2H is an A_i aromatic with one of its H atoms substituted with C_2H. A_i- denotes a radical formed from A_i and $A_iC_2H^*$ a radical of A_iC_2H with the unpaired electron located next to the C_2H group. P_2 represents biphenyl, an aromatic molecule with non-fused rings, whose importance was predicted for the conditions rich in benzene.[27] As will be demonstrated later in the text, the P_2-channel plays a key role under the conditions tested in the present study.

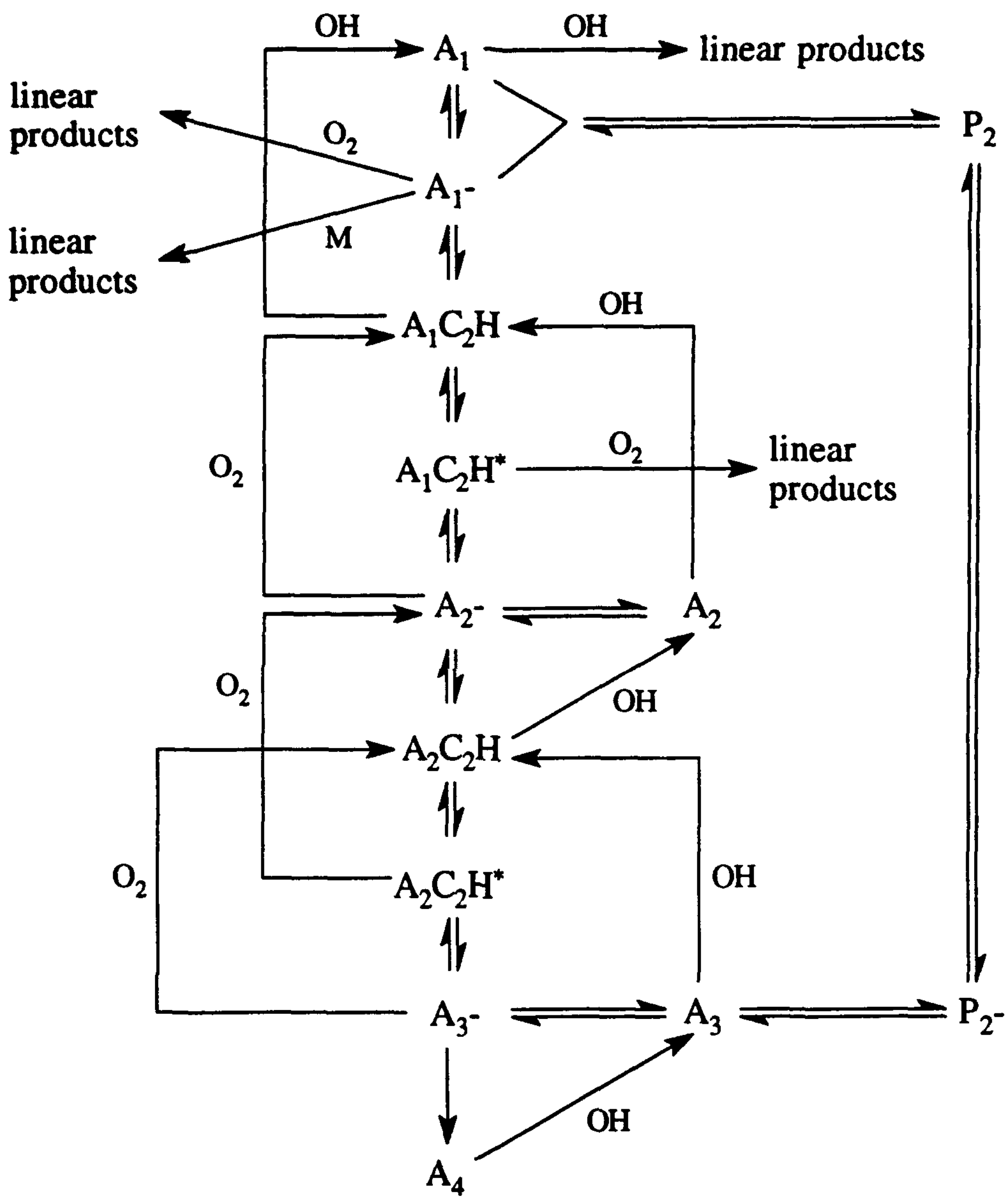

Figure 7. Reaction scheme of PAH growth.

TABLE 4. Mechanism of PAH growth.

No.	Reaction[a]	$k = AT^n e^{-E/RT}$ A ($cm^3mol^{-1}s^{-1}$)	n	E ($kJ\ mol^{-1}$)	References/ Comments
79.*i*	$A_i + H \rightleftharpoons A_i\text{-} + H_2$	2.50(+14)		66.9	*e,f*
80.*i*	$A_i + OH \rightleftharpoons A_i\text{-} + H_2O$	2.10(+13)		19.1	*e,g*
81.*i*	$A_i\text{-} + H \rightleftharpoons A_i$	5.80(-12)	8.29	−33.8	*h,i*
82.*i*	$A_i + OH \rightarrow$ products	1.00(+11)			*e,j*
83.*i*	$A_i\text{-} + O_2 \rightarrow$ products	2.00(+12)		31.3	*h,k*
84	$A_1\text{-} \rightarrow$ linear products	1.04(+29)	−4.26	324.0	*l*
85	$A_1\text{-} + C_2H_2 \rightleftharpoons A_1C_2H + H$	2.34(+34)	−5.71	129.4	*m*
86	$A_2\text{-} + C_2H_2 \rightleftharpoons A_2C_2H + H$	4.63(+31)	−5.05	123.0	*m*
87.*i*	$A_iC_2H^* + C_2H_2 \rightleftharpoons A_{i+1}\text{-}$	3.31(+50)	−10.95	112.8	*m,n*
88	$A_3\text{-} + C_2H_2 \rightarrow A_4 + H$	1.27(+44)	−8.71	138.2	*m*
89	$A_1 + A_1\text{-} \rightleftharpoons P_2 + H$	1.30(+03)	2.72	11.3	*o*
90	$P_2\text{-} + C_2H_2 \rightleftharpoons A_3 + H$	1.27(+44)	−8.71	138.2	$k_{90}=k_{88}$

[a] The rate coefficients for the reverse directions were determined via equilibrium constants. [e] A_i represents A_1, A_1C_2H, A_2, A_2C_2H, A_3 and P_2.[26] [f] Taken from Kiefer et al.[18] for the analogous reaction of benzene. [g] Taken from Madronich and Felder[19] for the analogous reaction of benzene. [h] A_i- represents A_1-, $A_1C_2H^*$, A_2-, $A_2C_2H^*$, A_3- and P_2-.[26] [i] Based on RRKM calculations for the phenyl and hydrogen atom association reactions at 10 bar with the parameters taken from Rao and Skinner.[20] The forward rate coefficient $k = AT^n\exp(-E/RT - 2.77\times10^{-3}\,T - 5.58\times10^{-7}\,T^2)$. [j] For $i = 1$ a linear hydrocarbon product is assumed; for $i > 1$ the product is an aromatic molecule with two carbon atoms less than A_i. The rate coefficient is estimated, see Ref. 1. [k] For $i = 1$ a linear product is assumed; for $i > 1$ the product is an aromatic radical with two carbon atoms less than A_i. The rate parameters were taken from Lin and Lin[21] for the analogous reaction of phenyl. [l] Assigned the rate coefficient of the ring opening reaction $A_1\text{-} \rightarrow n\text{-}C_6H_5$. [m] Based on RRKM calculations at 10 bar with parameters taken from Ref. 16. [n] $i = 1, 2$. [o] The rate coefficient expression was obtained using RRKM calculations, fitted to the experimental data of Fahr and Stein[28] and Scaiano and Stewart.[29]

Assuming steady state for all the radicals in the sequence shown in Fig. 7 and partial equilibrium for reactions (85) and (86) (see Table 4), we obtain an analytical expression relating the concentrations of pyrene and benzene,

$$\frac{d[\mathrm{A}_4]}{dt} = k_{88}[\mathrm{C_2H_2}]\left([\mathrm{A}_1]\prod_{i=1}^{7} B_i + B_1 E + D\right)$$

where

$$B_1 = k_{87}[\mathrm{C_2H_2}]\left\{k_{-87,2} + k_{88}[\mathrm{C_2H_2}] + k_{83}[\mathrm{O_2}] + Z_{2,5}k_{82}[\mathrm{OH}]/\left(Z_{1,5} + k_{82}[\mathrm{OH}]\right)\right\}^{-1}$$

$$B_2 = Z_{1,4}\left(Z_{2,4} + k_{87}[\mathrm{C_2H_2}] + k_{83}[\mathrm{O_2}] - k_{-87,2}B_1\right)^{-1}$$

$$B_3 = k_{86}[\mathrm{C_2H_2}]/\left(k_{-86}[\mathrm{H}]\right)$$

$$B_4 = k_{87}[\mathrm{C_2H_2}]\left(k_{-87,1} + k_{85}[\mathrm{O_2}] + Z_{2,3}\right)^{-1}$$

$$B_5 = Z_{1,2}\left(Z_{2,2} + k_{87}[\mathrm{C_2H_2}] + k_{83}[\mathrm{O_2}] - k_{-87,1}B_4\right)^{-1}$$

$$B_6 = k_{85}[\mathrm{C_2H_2}]/\left(k_{-85}[\mathrm{H}]\right)$$

$$B_7 = Z_{1,1}\left\{Z_{2,1} + k_{82} + k_{83}[\mathrm{O_2}] + Z_{1,6}\,k_{89}[\mathrm{A_1}]/\left[Z_{1,6} + k_{-89}[\mathrm{H}] + Z_{2,6}\,k_{-89}[\mathrm{H}]/\left(k_{88}[\mathrm{C_2H_2}]\right)\right]\right\}^{-1}$$

$$C = Z_{1,6}B_7k_{88}k_{89}[\mathrm{C_2H_2}][\mathrm{A_1}]^2\left\{Z_{1,6}k_{88}[\mathrm{C_2H_2}] + k_{-89}[\mathrm{H}]\left(Z_{2,6} + k_{88}[\mathrm{C_2H_2}]\right)\right\}^{-1} + k_{82}[\mathrm{OH}][\mathrm{A_4}]$$

$$D = Z_{1,5}C\left\{\left(k_{-87,2} + k_{88}[\mathrm{C_2H_2}] + k_{83}[\mathrm{O_2}]\right)\left(Z_{1,5} + k_{82}[\mathrm{OH}]\right) + Z_{2,5}k_{82}[\mathrm{OH}]\right\}^{-1}$$

$$E = k_{-87,2}D\left\{Z_{2,4} + k_{87}[\mathrm{C_2H_2}] + k_{83}[\mathrm{O_2}] - k_{-87,2}B_1\right\}^{-1}$$

$$Z_{1,i} = k_{79,i}[\mathrm{H}] + k_{80,i}[\mathrm{OH}] + k_{-81,i}$$

$$Z_{2,i} = k_{-79,i}[\mathrm{H_2}] + k_{-80,i}[\mathrm{H_2O}] + k_{81,i}[\mathrm{H}]\,.$$

The rate coefficients appearing in the above equations are given in Table 4 (reactions 79 – 90). They were obtained from RRKM calculations for a pressure of 10 bar and temperatures from 500 to 3000 K. The rate coefficients evaluated at 10 bar are within a factor of 2 from the values at 100 bar and were therefore assumed to be pressure independent in the present calculations.

The accuracy of the reduced model of PAH growth was tested by performing kinetic calculations on an individual fluid cell whose initial conditions are typical of those producing soot in high-pressure turbulent combustion. The results, shown in Fig. 8, indicate that the reduced model overpredicts the pyrene concentration in the beginning, but gets closer to it at times around 1 ms, the average cell reaction time. The difficulty of obtaining a more accurate reduced model for the reaction scheme in Fig. 7 resides in the complex behavior of A_2 and A_3. Assuming their formation irreversible and omitting the P_2 channel predicts well the initial part of the A_4 profile but greatly underpredicts it in the range of interest. Assuming A_2 is in a steady state or neglecting A_2 altogether overpredicts the A_4 concentration at all reaction times. The physical reason for this is the compound kinetics of A_2: it accumulates at first and then reacts at the later stages of reaction. A compromise solution was obtained by assuming the formation of A_2 irreversible, neglecting the formation of A_1C_2H in the oxidation of A_2 by OH, and including the P_2 channel, whose importance in this case was evident (compare, e.g., curve b with a in Fig. 8). In doing so, species P_2, P_2- and A_3 were assumed to be in steady state.

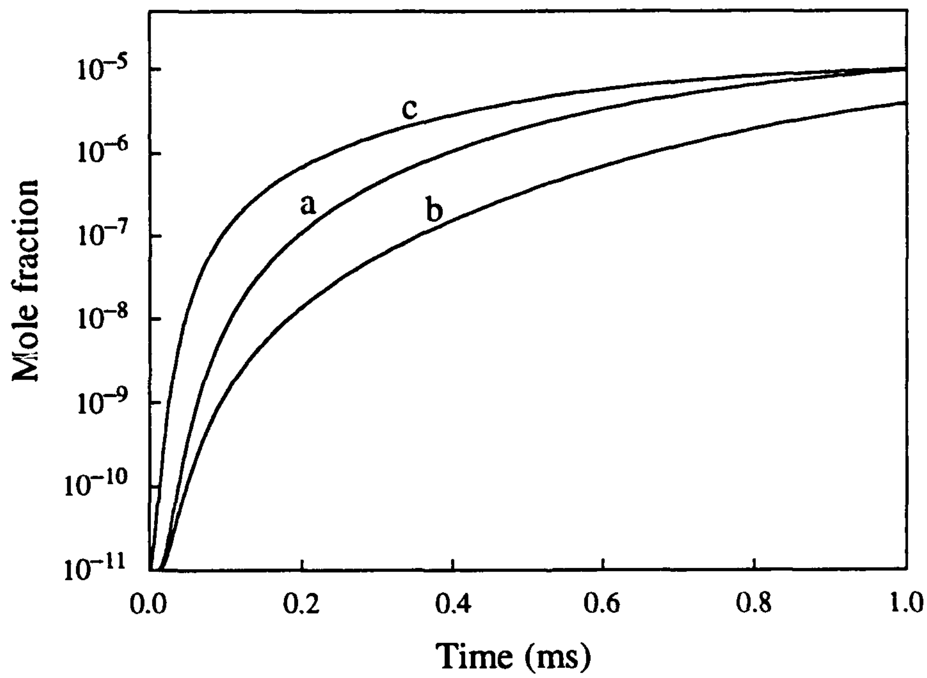

Figure 8. Calculated mole fraction of A_4 for the conditions of a single fluid cell: $P_0 = 39$ atm, $T_0 = 1954$ K, $\phi = 3.68$, and initial mole fraction of A_4 9.3×10^{-12}. a) Computed with the full reaction scheme for PAH growth (Fig. 7 and reactions 79 – 90 in Table 4). b) The same as (a) but without the P_2 reaction channel (i.e., without reactions 89 and 90). c) Computed with the reduced model of PAH growth.

PRINCIPAL CONCLUSIONS

The principal accomplishment of the last three-year period is the demonstration that the kinetic model developed for soot formation is capable of quantitative-level predictions for not only low-pressure laboratory flames, but also for more "practical" flames: sooting limits of laminar premixed flames,[1] soot profiles in high pressure flames,[30] and soot formation in turbulent combustion.[31]

New theoretical results provide further evidence against an ionic pathway for polycyclic aromatic precursors to soot in hydrocarbon flames.

New methods for estimation of thermodynamic and transport properties of polycyclic aromatic hydrocarbons were developed.

FUTURE WORK DIRECTION

Based on the success in modeling soot formation at high pressures, the direction for the future research under the currently renewed AFOSR-sponsored project is to attempt modeling of soot formation in environments even closer related to practical combustors, like diffusion and turbulent flames, along with further refinement of the underlying reaction mechanism of soot formation.

PRESENTATIONS AND PUBLICATIONS

Journal Articles

"A New Mechanism for the Formation of Meteoritic Kerogen-Like Material," W. A. Morgan, E. D. Feigelson, H. Wang, and M. Frenklach, *Science* **252**, 109-112 (1991).

"A Computational Study of Sooting Limits in Laminar Premixed Flames of Ethane, Ethylene and Acetylene," P. Markatou, H. Wang and M. Frenklach, *Combust. Flame* **93**, 467–482 (1993).

"Enthalpies of Formation of Benzenoid Aromatic Molecules and Radicals," H. Wang and M. Frenklach, *J. Phys. Chem.* **97**, 3867–3874 (1993).

"A Theoretical Study of Reaction between Phenylvinyleum Ion and Acetylene," H. Wang, B. Weiner and M. Frenklach, *J. Phys. Chem.* **97**, 10364–10371 (1993).

"Transport Properties of Polycyclic Aromatic Hydrocarbons for Flame Modeling," H. Wang and M. Frenklach, *Combust. Flame* **96**, 163–170 (1994).

Combustion Symposia

"Detailed Modeling of Soot Particle Formation and Growth," M. Frenklach and H. Wang, *Twenty-Third Symposium (International) on Combustion*, The Combustion Institute, Pittsburgh, 1991, pp. 1559–1566.

"Detailed Modeling of Soot Formation in Laminar Premixed Ethylene Flames at a Pressure of 10 Bar," A. Kazakov, H. Wang and M. Frenklach, *Twenty-Fifth Symposium (International) on Combustion*, Irvine, CA, July 31 – August 5, 1994, submitted.

"Reduced Mechanism of Soot Formation—Application to Natural Gas Fueled Diesel Combustion," by Y. Yoshihara, A. Kazakov, H. Wang and M. Frenklach, *Twenty-Fifth Symposium (International) on Combustion*, Irvine, CA, July 31 - August 5, 1994, submitted.

Chapters in Books

"Reduction of Chemical Reaction Models," M. Frenklach, in *Numerical Approaches to Combustion Modeling* (E. S. Oran and J. P. Boris, Eds.), Progress in Astronautics and Aeronautics, Vol. 135, American Institute of Aeronautics and Astronautics, Washington, D.C., 1991, pp. 129–154.

"Development of Chemical Reaction Models," M. Frenklach, in *Chemical Reactions in Complex Systems* (A. V. Sapre and F. J. Krambeck, Eds.), Van Nostrand Reinhold, 1991, pp. 197–221.

"Detailed Mechanism and Modeling of Soot Formation," M. Frenklach and H. Wang, in *Advanced Combustion Science* (T. Someya, Ed.), Springer-Verlag, Tokyo, 1993, pp. 168–175.

"Detailed Mechanism and Modeling of Soot Particle Formation," M. Frenklach and H. Wang, in *Mechanisms and Models of Soot Formation* (H. Bockhorn, Ed.), Springer-Verlag, Heidelberg, in press.

Invited Presentations

"Mechanism and Modeling of Soot Formation," M. Frenklach, Princeton University, Department of Mechanical and Aerospace Engineering, February 19, 1991, (Departmental seminar).

"Mechanism and Modeling of Soot Formation," M. Frenklach, HSR Chemical Kinetics Program Review Meeting, NASA-Lewis Research Center, Cleveland, OH, March 25, 1991.

"What are the Barriers to Modeling Soot Formation and Oxidation in Diesels and Gas Turbines?" M. Frenklach, ARO Conference on *Particulates in Heterogeneous Combustors*, Boulder, CO, June 12–13, 1991 (keynote).

"Aromatics Growth beyond the First Ring and the Nucleation of Soot Particles," M. Frenklach and H. Wang, Symposium on *Combustion Chemistry*, 202nd ACS National Meeting, New York, August 25–30, 1991 [*Preprints of the 202nd ACS National Meeting*, Vol. 36, No. 4, 1991, pp. 1509–1516].

"Aerosol Processes in Materials Science," M. Frenklach, American Association for Aerosol Research 1991 Annual Meeting, Traverse City, MI, October, 7–11, 1991 (plenary lecture).

"Detailed Mechanism and Modeling of Soot Particle Formation," M. Frenklach and H. Wang, International Workshop on *Mechanisms and Models of Soot Formation*, Heidelberg, September 29–October 2, 1991.

"Chemistry and Modeling of Soot Formation," M. Frenklach, University of Wisconsin, Madison, Department of Mechanical Engineering, November 12, 1991, (Hall Lecture seminar series).

"Chemistry of Particle Forming Systems," M. Frenklach, Engineering Foundation Conference on Vapor Phase Manufacture of Ceramics," Kona, Hawaii, January 12–17, 1992.

"The Chemistry and Modeling of Soot Formation," M. Frenklach, Caterpillar Inc., Engine Division Engineering, July 8, 1992."

"Mechanism of Soot Particle Formation," M. Frenklach, Scientific Conference on Obscuration and Aerosol Research, Aberdeen Proving Ground, MD, June 22–25, 1992.

"Modeling of Complex Chemical Processes: From Gas Phase to Surface," M. Frenklach, SEMATECH/NIST Workshop on Chemistry of CVD Processes in Semiconductor Manufacturing, National Institute of Standards and Technology, Gaithersburg, MD, September 29–30, 1992.

"An Overview of Surface Reactions Occurring During Carbon Deposition," M. Frenklach, The University of Akron, Department of Chemical Engineering, September 23, 1993, (Departmental seminar).

"Chemistry of Vapor Phase Manufacture of Films and Powders," M. Frenklach, Symposium "Tutorial on Materials Processing," AIChE National Meeting, St. Louis, Missouri, November 7–12, 1993.

"Grain Formation and Grain Growth in Stellar Environments," M. Frenklach, Workshop on Isotopic Anomalies, NASA Origins of Solar Systems Program: *Interstellar Grains in the Laboratory*, Washington University, St. Louis, MO, November 18–20, 1993.

Submitted Presentations

"A Computational Study of Sooting Limits in Laminar Premixed Ethane/Oxygen/Nitrogen Flames," P. Markatou, H. Wang and M. Frenklach, Twenty-Fourth Fall Technical Meeting of the Eastern Section of the Combustion Institute, 1991, Paper 10, 4 pp.

"Enthalpies of Formation of PAH Molecules and Radicals," H. Wang and M. Frenklach, *Combustion Fundamentals and Applications*, Joint Technical Meeting of the Central and Eastern States Sections of the Combustion Institute, 1993, pp. 655–659.

"Sterically-Resolved Modeling of PAH Growth using a Dynamic Monte Carlo Method," M. Frenklach, *Third International Conference on Chemical Kinetics*, Gaithersburg, MD, July 12–16, 1993.

"Detailed Modeling of Soot Formation in High-Pressure Laminar Premixed Flames," A. Kazakov, H. Wang and M. Frenklach, Fall Technical Meeting of the Eastern States Section of the Combustion Institute, Princeton, NJ, 1993, pp. 295–298.

"Detailed Kinetic Modeling of Aromatics Formation, Growth and Oxidation in Laminar Premixed Flames," H. Wang and M. Frenklach, Fall Technical Meeting of the Eastern States Section of the Combustion Institute, Princeton, NJ, 1993, pp. 299–302.

"RRKM Analysis of Aromatic Radical Reactions with Acetylene," H. Wang and M. Frenklach, Fall Technical Meeting of the Eastern States Section of the Combustion Institute, Princeton, NJ, 1993, pp. 455–458.

PROFESSIONAL PERSONNEL

Dr. Michael Frenklach — Principal Investigator
Dr. Brian Weiner — Participating Faculty
Dr. Penelope Markatou — Postdoctoral Scholar
Dr. Hai Wang — Graduate Student/Postdoctoral Scholar
Mr. Andrei Kazakov — Graduate Student

INVENTIONS

None.

REFERENCES

1. Markatou, P., Wang, H., and Frenklach, M., *Combust. Flame* **93**, 467 (1993).
2. Harris, M. M., King, G. B. and Laurendeau, N. M., *Combust. Flame* **64**, 99 (1986); **67**, 269 (1987).
3. Frenklach, M. and Wang. H., *Twenty-Third Symposium (International) on Combustion*, The Combustion Institute, Pittsburgh, 1991, p. 1559.
4. Wang, H. and Frenklach, M., *J. Phys. Chem.* **97**, 3867 (1993).
5. Disch, R. L., Schulman, J. M., and Peck, R. C., *J. Phys. Chem.* **96**, 3998 (1992).
6. Wang, H. and Frenklach, M., *Combust. Flame* **96**, 163 (1994).
7. Wang, H., Weiner, B., and Frenklach, M., *J. Phys. Chem.* **97**, 10364 (1993).
8. Calcote, H. F. and Gill, R. J., "Computer modeling of soot formation comparing free radical and ionic mechanisms," Final Report to AFOSR, TP-495, 1991.
9. Calcote, H. F. and Keil, D. G., *Combust. Flame* **74**, 131 (1988).
10. Gerhardt, Ph., and Homann, K. H., *Combust. Flame* 81, 289 (1990); *J. Phys. Chem.* **94**, 5381 (1990).
11. Mätzing, H., and Wagner, H. Gg., *Twenty-First Symposium (International) on Combustion*, The Combustion Institute, Pittsburgh, 1988, p. 1047.
12. Böhm, H., Hesse, D., Jander, H., Lüers, B. Pietscher, J., Wagner, H. Gg., and Weiss, M., *Twenty-Second Symposium (International) on Combustion*, The Combustion Institute, Pittsburgh, 1989, p. 403.
13. Bönig, M., Feldermann, Chr., Jander, H., Lüers, B., Rudolph, G., and Wagner, H. Gg., *Twenty-Third Symposium (International) on Combustion*, The Combustion Institute, Pittsburgh, 1991, p. 1581.
14. Böhm, H., Feldermann, Chr., Heidermann, Th., Jander, H., Lüers, B., and Wagner, H. Gg., *Twenty-Fourth Symposium (International) on Combustion*, The Combustion Institute, Pittsburgh, 1993, p. 991.
15. Frenklach, M., and Wang, H., in *Proceedings of the International Workshop on Mechanisms and Models of Soot Formation* (H. Bockhorn, Ed.), Springer-Verlag, Heidelberg, in press.
16. Wang, H., *Detailed kinetic modeling of soot particle formation in laminar premixed hydrocarbon flames*, Ph.D. Thesis, The Pennsylvania State University, Pennsylvania, 1992.
17. Kee, R. J., Grgar, J. F., Smooke, M. D., and Miller, J. A., *A Fortran Program for Modeling Steady Laminar One-Dimensional Premixed Flames*, Sandia National Laboratories Report No. SAND85–8240, 1985.
18. Kiefer, J. H., Mizerka, L. J., Patel, M. R., and Wei, H. C., *J. Phys. Chem.* **89**, 2013 (1985).
19. Madronich, S. and Felder, W., *J. Phys. Chem.* **89**, 3556 (1985).
20. Rao, V. S. and Skinner, G. B., *J. Phys. Chem.* **92**, 2442 (1988).

21. Lin, C.-Y. and Lin, M. C., Paper 7 presented at the Fall Technical Meeting of the Eastern States Section of the Combustion Institute, Gaithersburg, Maryland, November 1987.

22. Harris, S. J. and Kennedy, I. M., *Combust. Sci. Technol.* **59**, 443 (1988).

23. Neoh, K. G., Howard, J. B., and Sarofim, A. F., in *Particulate Carbon: Formation During Combustion* (D. C. Siegla and G. W. Smith, Eds.), Plenum, New York, 1981, p. 261.

24. Jander, H., personal communication, 1992.

25. Westmoreland, P. R., Howard, J. B., and Longwell, J. P., *Twenty-First Symposium (International) on Combustion*, The Combustion Institute, Pittsburgh, 1988, p. 773.

26. Frenklach, M., Yuan, T., and Ramachandra, M. K., *Energy Fuels* **2**, 462 (1988).

27. Frenklach, M., Clary, D. W., Gardiner, W. C., Jr., and Stein, S. E., *Twenty-First Symposium (International) on Combustion*, The Combustion Institute, Pittsburgh, 1988, p. 1067.

28. Fahr, A. and Stein, S. E., *Twenty-Second Symposium (International) on Combusiton*; The Combustion Institute, Pittsburgh, 1989, p. 1023.

29. Scaiano, J. C. and Stewart, L. C., *J. Am. Chem. Soc.* **105**, 3609 (1983).

30. A. Kazakov, H. Wang and M. Frenklach, *Twenty-Fifth Symposium (International) on Combustion*, submitted.

31. Y. Yoshihara, A. Kazakov, H. Wang and M. Frenklach, *Twenty-Fifth Symposium (International) on Combustion*, submitted.